Pharm Res (2015) 32:1045–1054
DOI 10.1007/s11095-014-1517-x

RESEARCH PAPER

Improved Pharmacokinetic and Biodistribution Properties of the Selective Urokinase Inhibitor PAI-2 (SerpinB2) by Site-Specific PEGylation: Implications for Drug Delivery

Kara Lea Vine • Sergei Lobov • Vineesh Indira Chandran • Nathanial Lachlan Ewart Harris • Marie Ranson

Received: 2 August 2014 / Accepted: 11 September 2014 / Published online: 18 September 2014
© Springer Science+Business Media New York 2014

ABSTRACT

Purpose Overexpression of the serine protease urokinase (uPA) is recognised as an important biomarker of metastatic disease and a druggable anticancer target. Plasminogen activator inhibitor type-2 (PAI-2/SerpinB2) is a specific uPA inhibitor with proven potential for use in targeted therapy. However, PAI-2 is rapidly cleared *via* the renal system which impairs tumor uptake and efficacy. Here we aimed to improve the pharmacological properties of PAI-2 by site-specific PEGylation.

Methods Several cysteine to serine substitution mutants were generated for PEGylation with PEG-maleimide (size range 12–30 kDa) and the physico-chemical and biochemical properties of the PEG-PAI-2 conjugates characterised. Radiolabeled proteins were used for evaluation of blood clearance and tissue uptake profiles in an orthotopic breast tumor xenograft mouse model.

Results PEGylation of the PAI-2^{C161S} mutant gave a predominant mono-PEGylated-PAI-2 product (~90%) with full uPA inhibitory activity, despite a significant increase in hydrodynamic radius. Compared to un-PEGylated protein the plasma half-life and AUC for PEG_{20}-PAI-2^{C161S} were significantly increased. This translated to a 10-fold increase in tumor retention after 24 h compared to PAI-2^{C161S}, an effect not seen in non-target organs.

Conclusions Our data underscores the potential for PEG_{20}-PAI-2^{C161S} drug conjugates to be further developed as anti-uPA targeted therapeutics with enhanced tumor retention.

KEY WORDS biodistribution · PAI-2/SerpinB2 · pharmacokinetics · polyethylene glycol (PEG), metastatic breast cancer

Electronic supplementary material The online version of this article (doi:10.1007/s11095-014-1517-x) contains supplementary material, which is available to authorized users.

K. L. Vine • S. Lobov • V. I. Chandran • N. L. E. Harris • M. Ranson (✉)
School of Biological Sciences, Illawarra Health and Medical Research Institute, University of Wollongong, Wollongong, NSW 2522, Australia
e-mail: mranson@uow.edu.au

ABBREVIATIONS

AUC	Area under the curve
BD	Biodistribution
ΔCD-loop	CD-loop deleterious mutant
EPR	Enhanced permeability and retention
ECM	Extracellular matrix
i.v.	Intravenous
ID/g	Injected dose per gram
IEC	Ion exchange chromatography
MALDI TOF – MS	Matrix-assisted laser desorption/ionization time-of-flight – mass spectrometry
PK	Pharmacokinetic
PAI-2	Plasminogen activator inhibitor type-2
PEG	Polyethylene glycol
uPA	Urokinase plasminogen activator
uPAR	Urokinase plasminogen activator receptor

INTRODUCTION

Uncontrolled, overexpression of the urokinase plasminogen activation (uPA) system plays a key role in tumor invasion and metastasis by facilitating an increased ability of both tumor and tumor-associated cells to generate the highly destructive proteolytic enzyme plasmin and breakdown tissue barriers (1,2). Urokinase is synthesized and released in circulation as a zymogen (pro-uPA) whose activation is largely dependent and markedly accelerated upon binding to specific cell-surface uPA receptors (uPAR). Receptor-bound uPA activates plasminogen at the cell surface and thus promotes tissue degradation and remodelling of the local extracellular environment (3,4). This is achieved by initiating a cascade of pericellular, proteolytic events which can directly and indirectly (*via* activation of pro-metalloproteases; MMPs) degrade integral extracellular matrix (ECM)

molecules. Further, plasmin can activate various growth factors and cytokines leading to the induction of signalling events responsible for increased chemoattraction, cell migration and metastasis (5). Elevated cell surface uPA is now proven to be a critical marker of invasion and metastasis in most solid tumors and is the only breast cancer marker with level 1 (highest) evidence for a poor prognosis (6–8). uPAR is also expressed in the tumor stroma which translates to an aggressive tumor phenotype and poor relapse-free survival (2,9). Thus, uPA/uPAR represents a selective target for the development of anti-tumor/metastasis treatments (2,10,11).

Binding of cell surface, receptor bound uPA by the specific uPA inhibitor plasminogen activator inhibitor type-2 (PAI-2, SerpinB2) results in receptor-mediated endocytosis of the uPAR/uPA:PAI-2 complex (12–15). PAI-2 is thus able to efficiently and specifically deliver and concentrate covalently-bound therapeutic molecules within targeted cells. Previously, we have shown both wild-type and mutant forms of PAI-2 to preferentially target cytotoxins (16,17) and therapeutic radionuclides (18,19) to uPA-positive metastatic cancer cells *in vitro* and *in vivo*. Wild-type PAI-2 (47 kDa, non-glycosylated) contains a unique 33 amino acid loop between α-helices C and D (CD-loop) (6). This loop may be involved in secondary molecular interactions (20), yet is not required for the inhibitory function of PAI-2 and does not impact on the endocytosis properties of the uPAR/uPA:PAI-2 complex

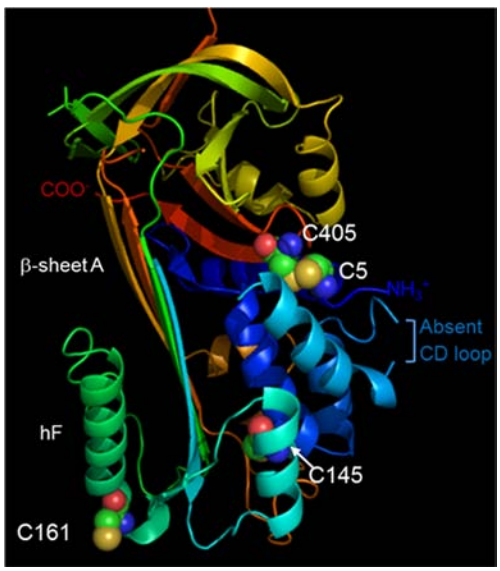

Fig. 1 The X-ray crystal structure of PAI-2 Δ CD-loop. The serpin molecule contains nine α-helices and three β-sheets with a mobile reactive centre loop (RCL) protruding from the dominant β-sheet A at the top of the molecule (not shown). Cysteine residues at positions 5, 145, 161 and 405 are shown as spheres on ribbon backbone colored in rainbow from amino (*indigo*) to carboxy (*red*) terminus. Amino acid numbering corresponds that of wild-type PAI-2. hF = alpha helix F. Structure coordinates are from PDB ID 1BY7 (34); the figure was produced using PyMOL (www.pymol.org).

(20,21). Thus, recombinant PAI-2 CD-loop deleterious mutant (PAI-2 ΔCD-loop; ~44 kDa; Fig. 1) serves as a good platform for further molecular modifications of PAI-2 that is designed solely for uPA targeting. PAI-2 is also non-immunogenic and is highly stable in the circulation; however its permanence in the body is limited by rapid renal elimination resulting in a low total dose reaching the tumor (22,23). Although this excretion profile is ideal for diagnostic tumor imaging; it is important to further increase the tumor uptake of PAI-2 in order its potential as a therapeutic delivery agent.

Several approaches exist to modulate the pharmacokinetic (PK) and biodistribution (BD) profiles of peptides and proteins to prolong circulation time in the body. The most common method involves conjugation to a polymer such as polyethylene glycol (PEG) (24–26). The hydrophilic nature of PEG creates a protective water shell around the coupled protein and as a result increases the residence time of the drug in the blood stream, thereby increasing bioavailability and clinical potency (25,27). PEGylation also offers additional advantages such as increased molecule solubility and stability (physical and thermal), protection against enzymatic degradation, decrease in clearance time (due to retardation of renal clearance) and reduced immunogenicity and toxicity (26). Coupling of PEG to polypeptides is most often achieved through conjugation to primary amine, carboxyl or thiol groups. Notably, the shape and number of PEG moieties attached affects the stability and efficacy of the drug conjugate (25). PEG location is therefore critical as non-specific PEGylation, particularly near the active site can result in an overall reduction in protein bioactivity. Site-specific PEGylation can therefore be achieved through the introduction of cysteine residues by genetic engineering, a strategy that offers fewer, more precise sites for PEG attachment and ultimately reduces heterogeneity whilst preserving activity (25). Human PAI-2 ΔCD-loop has four native cysteines in positions 5, 145, 161 and 405 (Fig. 1), none of which are required for the inhibitory function of the protein (28). These residues are therefore amenable to mutagenesis for the purpose of introducing groups that react chemoselectively with maleimide functionalized PEG.

In this study, different cysteine to serine substitution mutants were created on the PAI-2 ΔCD-loop backbone. Purified recombinant mutant protein was used for site-directed PEGylation in an overall effort to improve the pharmacological properties of PAI-2. Four recombinant mutants; PAI-2 ΔCD-loop, PAI-2 ΔCD-loop C145S, PAI-2 ΔCD-loop C161S and PAI-2 ΔCD-loop C5/145/405S (referred to as PAI-2, PAI-2^{C145S}, PAI-2^{C161S} and PAI-$2^{C5/145/405S}$, respectively hereafter) were PEGylated with three different sized PEG molecules (12 kDa, 20 kDa and 30 kDa PEG) and their physico-chemical and uPA inhibitory activity properties

assessed. Finally the PK, BD and tumor uptake properties of ^{125}I-PAI-2^{C161S} and ^{125}I-PEG$_{20}$-PAI-2^{C161S} were compared in an orthotopic, breast tumor xenograft mouse model.

MATERIALS AND METHODS

Reagents

All chemicals were purchased from Sigma-Aldrich unless otherwise indicated. The pQE9 vector and M15[pREP4] *E. coli* were obtained from QIAgen; Oligonucleotides were purchased from Sigma-Genosys. QuikChange site-directed mutagenesis kit was from Stratagene (La Jolla, CA). L21 Star (DE3) *E. coli* was from Invitrogen and IPTG from Applichem. High molecular weight (HMW)-uPA from American Diagnostica; Ampicillin and kanamycin from Amresco; TALON metal affinity resin from Clontech; *Bam*HI restriction enzyme, shrimp alkaline phosphatase and T4 DNA ligase from Fermentas. Pfu HS Fusion II DNA polymerase was purchased from Stratagene, PD-10 desalting columns from GE BioSciences. Methoxy polyethylene glycol (PEG) maleimide (with molecular weights of 12 kDa, 20 kDa and 30 kDa, PEG$_{12–30}$) were purchased from NOF Corporation (Japan). Na-^{125}I was purchased from PerkinElmer and EDTA animal blood tubes were obtained from Interpath Services Pty Ltd.

Mutagenesis

For simplicity we refer to the PAI-2 ΔCD-loop mutant and its derivatives as PAI-2 unless otherwise specified. Note that amino-acid numbering within the PAI-2 mutants corresponds to that of the wild-type PAI-2. Generation of the single mutants PAI-2 ΔCD-loop C145S (PAI-2^{C145S}) and PAI-2 ΔCD-loop C161S (PAI-2^{C161S}), and triple mutant PAI-2 ΔCD-loop C5/145/405S (PAI-2$^{C5/145/405S}$) were performed by site-directed mutagenesis of pQE9/PAI-2 ΔCD-loop (PAI-2) as previously described (21). Expression and purification of all mutants was performed using the pQE9 vector system as previously described (21). All mutants were confirmed to retain their inhibitory activity as determined by the formation of high molecular weight complexes with uPA (data not shown).

PEGylation of PAI-2 and PAI-2 Mutants

PEGylation reactions were performed according to the manufacturer's instructions with minor modifications. Briefly, DTT reduced or non-reduced PAI-2, PAI-2^{C145S}, PAI-2^{C161S} and PAI-2$^{C5/145/405S}$ (>1 mg/mL) in PBS (pH 7.4) were reacted with 20–40-fold M excess of activated PEG (in dH_2O) for 2–4 h at RT (with shaking), then at 4°C overnight (unless otherwise stated). Samples were assessed for degree of PEGylation by 10% SDS-PAGE under reducing conditions and visualized after staining with Coomassie blue. Relative abundance was calculated by densitometry (ImageJ 1.45 Software, NIH). The ability of PEG-PAI-2 to form covalent, SDS-stable complexes with uPA was confirmed after incubating the various PEG-PAI-2 conjugates with HMW uPA (2:1) at 37°C for 10 min as previously described (21) then fractionating by SDS-PAGE as described above.

Purification of PEG-PAI-2^{C161S} by Ion Exchange Chromatography (IEC)

Purification of PEGylated PAI-2^{C161S} was performed on the AKTA Purifier (UNICORN 5.01) using a Hi Screen Capto Q ImpRes anion exchange column. The PEG$_{20}$-PAI-2^{C161S} conjugate was bound to the column in 20 Tris–HCl, pH 8.0 and eluted in fractions with 500 mM NaCl over 60 min at a flow rate of 0.5 mL/min. The concentration of PAI-2 in the collected fractions was determined by Lowry assay.

Matrix-assisted Laser Desorption/Ionization Time-of-Flight—Mass Spectrometry (MALDI TOF—MS)

Sample Preparation

The MALDI TOF analyses of PAI-2^{C161S} and PEG$_{20}$-PAI-2^{C161S} were performed according to the method described by Seyfried *et al.* (29) with slight modifications. Firstly, for matrix preparation, a mixture of acetonitrile, dH_2O and trifluoroacetic acid in 40:60:0.1 ratio was added to a matrix aliquot of sinapinic acid to achieve a final concentration of 10 mg/mL. The mixture was mixed thoroughly by vortexing for 30 s and then spun in a microcentrifuge at 14,000 rpm to separate undissolved matrix and the supernatant was used for further analysis. For sample preparation in the case of PAI-2^{C161S}, after the deposition of 0.5 μL of matrix solution onto the target plate, approximately 0.5 μL of PAI-2^{C161S} in 10 mM Tris buffer (pH 8.0) was injected onto the matrix droplet and dried at RT. For PEG$_{20}$-PAI-2^{C161S}, approximately 1 μL of matrix and 1 μL of PEG$_{20}$-PAI-2^{C161S} in 10 mM Tris buffer (pH 8.0) were mixed thoroughly in an eppendorf tube and 1 μL of the homogeneous solution was deposited on the target plate and dried at RT.

Analyses

All measurements were performed in the linear positive ion mode with an AXIMA Confidence instrument (Shimadzu Biotech, Manchester, UK) equipped with a nitrogen laser and applying a source voltage of 20,000 V, einzel lens voltage of 6,500 V, pulsed extraction voltage of 2,625 V, reflectron voltage of 24,400 V, linear detector voltage of 2,700 V, and reflection detector voltage of 1,850 V. All analyses were

performed by Dr. David Harman (NMR and MS Manager, ARC Centre of Excellence for Electromaterials Science, Intelligent Polymer Research Institute, University of Wollongong) using the Shimadzu Biotech Axima Confidence software (version 2.8.3).

Fluorogenic uPA Activity Assay

Various concentrations of PAI-2^{C161S} and $PEG_{12\text{-}30}$-PAI-2^{C161S} [to give molar ratios of 5 –0.31:1 (PAI-2:uPA)] were diluted in reaction buffer (20 mM HEPES, pH 7.6, 100 mM NaCl, 0.5 mM EDTA, 0.01% (v/v) Tween 20) and mixed with fluorogenic substrate, Z-Gly-Gly-Arg-AMC in 180 µL reaction buffer (final concentration 0.25 mM). After a brief pre-incubation at 37°C, high molecular weight two-chain active uPA (final concentration 0.75 nM) was added to start the reaction and fluorescence emission measured immediately at 37°C over 1 h. All assays were performed in triplicate and values corrected by subtracting the background (reaction buffer plus substrate only).

Radioiodination of Proteins

Recombinant human PAI-2^{C161S} and PEG_{20}-PAI-2^{C161S} were radiolabelled with Na-^{125}I using the iodo-bead procedure and purified as previously described (22). ^{125}I-PAI-2 preparations were stored at 4°C and used in experiments within two weeks of iodination. Inhibitory activity of ^{125}I-PAI-2^{C161S} and ^{125}I-PEG_{20}-PAI-2^{C161S} was confirmed by their ability to form uPA:PAI-2 complexes as detected by SDS-PAGE and autoradiography (data not shown).

Cell Lines and Animals

MDA-MB-231 human breast carcinoma cells were purchased from American Type Culture Collection (ATCC; USA, distributed by Cryosite, Australia) and routinely cultured in RPMI-1640 supplemented with 5% heat inactivated FCS at 37°C under a 5% CO_2, 95% atmosphere. Cell viability and cell number were assessed prior to experimentation using the Trypan blue (Sigma-Aldrich) exclusion method, with viable cells counted using a haemocytometer. Cell lines were routinely tested for Mycoplasma contamination and found to be negative. Expression of cell surface uPAR, uPA and triple negative tumor status was verified by indirect immunofluorescence using dual color flow cytometry or western blotting as previously described (30). SPF-bred Balb/c nu/nu mice were obtained from the Animal Resources Centre (Canning Vale, WA, Australia) and were housed in a ventilated storage cabinet under positive pressure in autoclaved filter-top cages. Animal experiments were performed in compliance with the NHMRC Australian Code of Practice for the care and use of animals for scientific purposes and sanctioned by the University of Wollongong Animal Care and Ethics Committee. Orthotopic breast carcinoma xenografts were established by subcutaneous injection of 1×10^6 MDA-MB-231 cells into the first, left mammary fat pad of 5 week old female Balb/c nu/nu mice and have been shown to express uPA/uPAR (19). Tumors were allowed to grow to approximately 300 mm^3 in volume (4 weeks post injection of tumor cells) and animals randomly allocated into groups.

Biodistribution (BD) and Pharmacokinetics (PK) of PEG_{20}-PAI-2^{C161S}

BD and PK studies were conducted in mice 4 weeks after tumor cell inoculation. Animals were injected intravenously (i.v.) with a single bolus dose of 2 µCi (74 kBq) of ^{125}I-PEG_{20}-PAI-2^{C161S} or ^{125}I-PAI-2^{C161S} through the lateral tail vein and sacrificed by overdose of CO_2 between 10 min and 24 h after injection. Blood was immediately collected into tubes containing EDTA and plasma samples taken after centrifugation (2,000 rpm, 15 min) on a bench-top microcentrifuge (5415C, Eppendorf). Major organs (*i.e.* liver, spleen and kidneys) and the tail (for dose correction) were collected and weighed for further tissue/organ analysis. Radioactivity in each sample was measured with a γ-counter (Wizard™ 3, Perkin Elmer). The percentage of the injected dose (% ID) in the organs was calculated by comparison to suitable dilutions of the ^{125}I-PEG_{20}-PAI-2^{C161S} or ^{125}I-PAI-2^{C161S} stock. The % ID per gram (% ID/g) of tissue was found by dividing the % ID for each organ by the weight of the organ and corrected for the amount of radioactivity remaining in the tail. Blood clearance (PK) profiles were determined by plotting the % ID remaining in the blood over time post radiotracer injection and fitted to a two phase exponential decay model using GraphPad Prism V 5.1 for Windows (GraphPad Software, San Diego CA USA). Due to the use of tracer doses of ^{125}I-PAI-2^{C161S} and ^{125}I-PEG_{20}-PAI-2^{C161S} we did not quantify the amount of intact/catabolized exogenous PAI-2 in this study. Four mice were used for each time point. The average tumor volume of mice receiving ^{125}I-PAI-2^{C161S} or ^{125}I-PEG_{20}-PAI-2^{C161S} was 314.2 mm^3 (±44.12) and 316.1 mm^3 (±42.04), respectively.

Statistical Analysis

Statistical significance of treatment groups as compared to control groups was determined using a two-way ANOVA with a Bonferroni post-test or unpaired students multiple *t* test with correction for multiple comparisons using the Šídák-Bonferroni method (GraphPad Prism V 6.0; San Diego, CA, USA). P values < 0.05 were considered statistically significant.

RESULTS

Site-directed PEGylation of PAI-2^{C161S} Results in a Predominant Mono-PEGylated Product

Site-directed PEGylation of the PAI-2 mutants C161S, C145S and C5/145/405S with 12, 20 and 30 kDa PEG was achieved by reaction of purified PAI-2 with activated maleimide derivatives of the polymer. The degree of PEGylation was different for each mutant, such that PAI-2^{C161S} yielded a major mono-PEGylated product (>91%) with a molecular weight of 57 kDa (Fig. 2), while PAI-2 and PAI-2^{C145S} generated a heterogeneous population of PEG-PAI-2 species, with up to 4 PEG attachments per molecule detected (Fig. 2). The most abundant protein species found for PAI-2 and PAI-2^{C145S} was tri-PEGylated (55 and 71%, respectively). Reducing PAI-2^{C161S} with DTT prior to PEGylation found no difference in the proportion of PEG-PAI-2 species obtained, irrespective of the size of the PEG moiety attached (Fig. S1, Supplementary Information). Covalent attachment of PEG to the triple mutant PAI-2$^{C5/145/405S}$, containing only a single cysteine at position 161, improved upon the PEGylation profile of PAI-2^{C145S} as a predominant mono-PEGylated species was obtained (Supplementary Information, Fig. S2). However, since the single mutant PAI-2^{C161S} also produced a mono-PEGylated product in high yield, and contained fewer amino acid residue modifications, this mutant was utilized for subsequent investigations.

Purification of PEG$_{20}$-PAI-2^{C161S} by Ion Exchange Chromatography (IEC) and Confirmation of PEG Attachment by MALDI-TOF MS

Mono-PEGylated PAI-2^{C161S} conjugates were further purified to homogeneity using ion exchange chromatography. Three charged PAI-2^{C161S} species (peaks 1-3; Fig. 3a) were detected by IEC after PEGylation with 20 kDa PEG. Mono-PEGylated PAI-2^{C161S} eluted as a single major peak (peak 2; Fig. 3a) over 3 fractions, while di-PEGylated-PAI-2^{C161S} (peak 1; Fig. 3a) eluted immediately prior to mono-PEGylated-PAI-2^{C161S} and un-PEGylated-PAI-2^{C161S} (peak 3; Fig. 3a) eluted immediately after. The order of elution was dependent on a decrease in the dynamic binding capacity of the species due to i) changes in the relative negative charge density on these species caused by the neutral PEG chain and ii) the increased mass transfer resistance associated with the large size of the PEG molecule (31) (di-PEG-PAI-2^{C161S}<mono-PEG-PAI-2^{C161S}<PAI-2^{C161S}) (Fig. 3b, Lanes 5–10). MALDI-TOF MS analysis of purified PEG$_{20}$-PAI-2^{C161S} fractions obtained from IEC confirmed the attachment of one (65,795.9 Da) (Fig. 3d) and two (86,633.5 Da) (Fig. 3e) 20 kDa PEG moieties per PAI-2^{C161S} molecule.

PEG-PAI-2 Conjugates Retain uPA Inhibitory Activity

All PAI-2 mutants and PEG-PAI-2 conjugates formed SDS-stable complexes with uPA (see Supplementary Information Fig. S2 for representative examples). The inhibitory capacity of PEG-PAI-2^{C161S} was quantitated using a fluorescence-based uPA activity assay. No significant differences between PEG$_{12\text{-}30}$-PAI-2^{C161S} and unPEGylated PAI-2^{C161S} were observed across a range of molar concentrations as determined by two-way ANOVA (Fig. 4). At a molar ratio of 0.6:1 (PAI-2:uPA) the percent inhibition of total uPA activity decreased as the size of the PEG moiety attached increased, however this finding was not statistically significant. Altogether, these results confirm that modification of cysteine residues by either site-directed mutagenesis and/or PEGylation does not compromise the inhibitory activity of PAI-2.

Tumor Retention of PEG$_{20}$-PAI-2^{C161S} is 10-times Greater than PAI-2^{C161S} at 24 h

The PK and BD profiles of ^{125}I-PAI-2^{C161S} and ^{125}I-PEG$_{20}$-PAI-2^{C161S} were determined over 1,440 min (24 h) after a single i.v. administration to Balb/c nude mice bearing MDA-MB-231 breast carcinoma xenografts. PK parameters were calculated from a two-phase exponential decay model and are summarized in Table I. The plasma clearance profiles of the two proteins were significantly different with ^{125}I-PEG$_{20}$-PAI-2^{C161S} exhibiting a decrease in both the initial rate of drug distribution (K_{elim} $\alpha = 0.06 \pm 0.04$ min^{-1} vs 0.02 ± 0.01 min^{-1}) and drug elimination (K_{elim} $\beta = 0.001 \pm 0.001$ min^{-1} vs 0.002 ± 0.001 min^{-1}) compared to ^{125}I-PAI-2^{C161S} (Fig. 5). This translated to a 3-fold increase in the distribution half-life ($T_{1/2}$ $\alpha = 31.4$ min vs 11.6 min) and a 2-fold increase in the terminal half-life ($T_{1/2}$ $\beta = 708$ min vs 426 min) of the PEGylated protein in the plasma. The area under the curve (AUC) for ^{125}I-PEG$_{20}$-PAI-2^{C161S} was 5-times greater than for ^{125}I-PAI-2^{C161S} (38,674 vs 7,537% ID/min/mL, respectively). Likewise, the maximum concentration (C_{max}) of radioactivity in the plasma after ^{125}I-PEG$_{20}$-PAI-2^{C161S} injection was significantly higher ($P = 0.0024$) than for unPEGylated protein. By 1,440 min, < 1% *versus* 12% of the radioactivity remained in the plasma of mice injected with ^{125}I-PAI-2^{C161S} compared to ^{125}I-PEG$_{20}$-PAI-2^{C161S}, respectively (Fig. 5).

Analysis of the BD patterns of major organs found that kidneys accumulated the highest radioactivity levels, followed by the liver and then the spleen and that this occurred within the first 10 min after injection of either ^{125}I-PAI-2^{C161S} or ^{125}I-PEG$_{20}$-PAI-2^{C161S} into mice (Table II). The % ID/g tissue for PAI-2^{C161S} was on average 2 times higher than that for PEG$_{20}$-PAI-2^{C161S} in all organs at this peak time point (Table II). For both forms radioactivity levels declined thereafter in all organs with no significant differences in

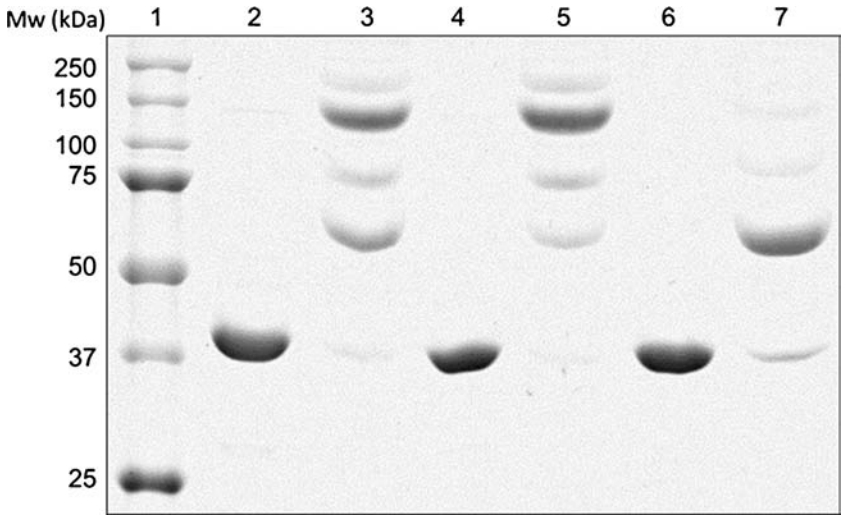

Fig. 2 Site-directed PEGylation of PAI-2 ^{C161S}. Native and cysteine substitute mutants of PAI-2 (PAI-2^{C145S} and PAI-2^{C161S}) were PEGylated with a 20-fold molar excess of 12 kDa PEG (PEG_{12}), fractionated under reducing conditions using 10% SDS PAGE and visualized after staining with Coomassie blue. *Lane 1*: mw markers, *Lane 2*: PAI-2, *Lane 3*: PEG_{12}-PAI-2, *Lane 4*: PAI-2^{C145S}, *Lane 5*: PEG_{12}-PAI-2^{C145S}, *Lane 6*: PAI-2^{C161S}, *Lane 7*: PEG_{12}-PAI-2^{C161S}. Non-PEGylated PAI-2 accounted for less than 10% of the protein detected in all cases.

radioactivity levels observed between the two treatment groups from 180 min after injection.

Radioactivity levels in tumors peaked at 60 min (4.66± 0.51% ID/g) and 180 min (3.94±0.41% ID/g) after injection of ^{125}I-PAI-2^{C161S} and ^{125}I-PEG_{20}-PAI-2^{C161S}, respectively, though peak levels were not significantly different from each other (Table II). Radioactivity levels decreased significantly between 360 and 1,440 min (24 h) in tumors of mice treated with ^{125}I-PAI-2^{C161S}, with the majority (99.8%) of radioactivity cleared from the tumors by the end of the observation period. This decline was much less apparent in tumors of mice treated with ^{125}I-PEG_{20}-PAI-2^{C161S}. While overall tumor uptake was not significantly different between treatments as determined by AUC values (10–1,440 min), the trend favours uptake of PEGylated protein with 10 times the radioactivity level remaining in the tumors of mice treated with ^{125}I-PEG_{20}-PAI-2^{C161S} compared to ^{125}I-PAI-2^{C161S} 24 h after injection (Table II; Supplementary Information, Fig. S3).

DISCUSSION

The inappropriate, up-regulated expression of the uPA system plays a key role in tumour invasion and metastasis and is now recognised as having strong prognostic relevance in node negative breast cancer as well as being a therapeutic target (2,6,11). PAI-2 is highly selective uPA inhibitor and a number of studies have shown promising results using PAI-2 for the delivery of radioisotopes and cytotoxins in anti-uPA targeted therapy using (16,17,19,32). However, PAI-2 is rapidly cleared *via* the renal system which results in low tumour uptake (22). Previous work by our group comparing the pharmacological properties of PAI-2 using different radiolabelling methods also undertook preliminary analyses of a 2.5 kDa branched-chain ^{123}I-PEGylated PAI-2 ΔCD-loop derivative which resulted in modest increases in blood retention time and tumor uptake (23). This suggested that further modifications with larger PEG molecules could improve the accrual of PAI-2 in the tumor as it is widely reported that the bioavailability of PEGylated proteins and peptides increases with the size and/or number of PEG moieties attached (27,33). The current study validates this approach and lends weight to the further development of PEGylated PAI-2 as a therapeutic or diagnostic agent targeting the metastatic biomarker uPA.

The degree of PAI-2 PEGylation appeared to be directly proportional to the number of cysteine residues *accessible* for conjugation. PAI-2 lacking the CD-loop has four cysteine residues at positions 5, 145, 161 and 405; cysteines at positions 5 and 405 are buried deep within the molecule and are typically disulfide bonded (Fig. 1) (28,34). In agreement with this, PEGylation of the various PAI-2 mutants with 12, 20 or 30 kDa PEG found the single mutant PAI-2^{C161S} (containing cysteine residues at 5, 145 and 405), to yield a predominant mono-PEGylated product, presumably at C145. Reducing PAI-2^{C161S} prior to PEGylation did not alter this result, suggesting that the cysteine to serine mutation at position 161 leads to molecular stability of the modified protein, thus maintaining the inaccessibility of C5 and C405 under reducing conditions. Conversely, PEGylation of PAI-2 or the single PAI-2^{C145S} mutant, lead to the generation of a heterogeneous population of mono-, di- and tri-PEGylated species, where> 50% contained 3 PEG moieties/protein. Since C161 sits on

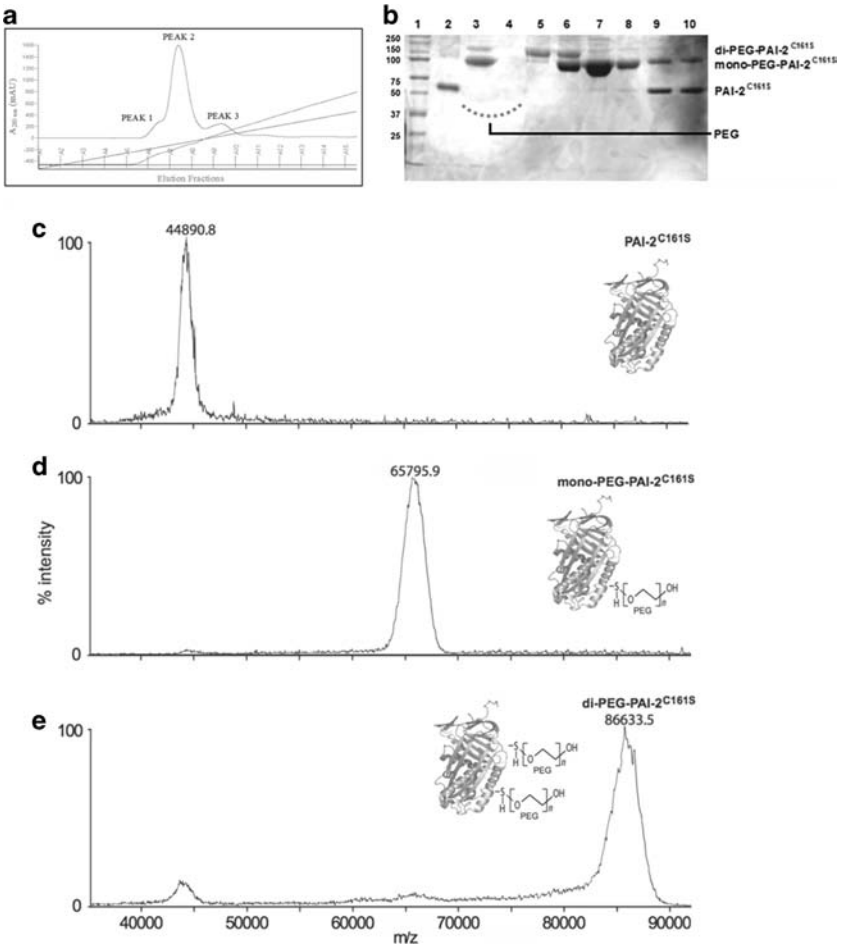

Fig. 3 Purification and characterization of PEG_{20}-PAI-2^{C161S}. (**a**) PEG_{20}-PAI-2^{C161S} was injected onto a Hi Screen Capto Q ImpRes anion exchange column and eluted using a linear NaCl gradient (0–500 mM) (100% B) at a flow rate of 0.5 mL/min. *Blue line*: elution of protein at 280 nm, *light green line*: NaCl concentration, *light blue*: percent conductivity, *dark green line*: relative pressure in the column. Peaks 1, 2, and 3 represent the elution of di-PEGylated, mono-PEGylated and unPEGylated PAI-2 species, respectively. (**b**) SDS-PAGE showing different elution fractions of PEG_{20}-PAI-2^{C161S} after purification using IEC. Samples were resolved under non-reducing conditions using a 10% SDS-PAGE and visualized by staining with Coomassie blue. *Lane 1*: mw markers, *Lane 2*: PAI-2^{C161S}, *Lane 3*: unpurified PEG_{20}-PAI-2^{C161S}, *Lanes 4–10*: elution fractions from IEC (approximately 4 μg protein loaded per lane). (**c**–**e**) MALDI-TOF MS of PEG_{20}-PAI-2^{C161S}. The average molecular weight of un-PEGylated PAI-2^{C161S} was calculated at 44,890.8 Da (**c**), PAI-2^{C161S} + 1 × 20 kDa PEG = 65,795.9 Da (**d**) and PAI-2^{C161S} + 2 × 20 kDa PEG = 86,633.5 Da (**e**).

helix F (Fig. 1), which is moderately mobile when the CD-loop is absent (35), we predict that the attachment of bulky PEG groups to cysteine at this position leads to molecular rearrangements that promote exposure of C5 and C405 for

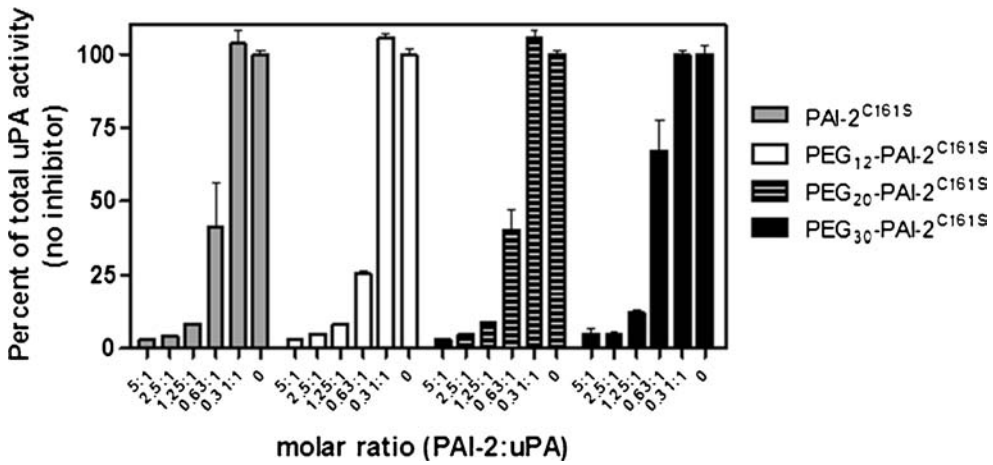

Fig. 4 PEGylated PAI-2 retains uPA inhibitory activity against uPA. The uPA fluorogenic substrate was briefly pre-incubated with various molar ratios of the PAI-2 forms or buffer alone and the assays initiated by the addition of uPA. Fluorescence units were converted to a percentage of the maximal (uninhibited) uPA activity. Values shown are the means of triplicate determinations ± SD.

Table I Comparison of the Pharmacokinetic (PK) Parameters of Radioiodinated PAI-2^{C161S} and PEG_{20}- PAI-2^{C161S} in the Plasma of Mice After i.v. Administration

PK parameters[a]	^{125}I-PAI-2^{C161S}	^{125}I-PEG_{20}- PAI-2^{C161S}
[b]C_{max} (% ID/mL)	32.2 (±6.75)	79.1 (±3.38)
[c]K_{elim} α (fast) min^{-1}	0.0596 (±0.0358)	0.0221 (±0.00670)
K_{elim} β (slow) min^{-1}	0.00163 (±0.000350)	0.000980 (±0.000148)
[d]$T_{1/2}$ α (fast) min	11.6	31.4
$T_{1/2}$ β (slow) min	426	708
Correlation coefficient (R^2)	0.980	0.971
[e]AUC (% ID/min/mL)	7,537	38,674

[a] Values (3 sig. fig.) were calculated using a two-phase exponential decay model using GraphPad Prism V6.0 software from data shown in Fig. 5

[b] C_{max} maximum plasma concentration. *Note*: T_{max} (the time required to reach C_{max}) = 0 for i.v. administration

[c] K_{elim} α distribution rate constant, K_{elim} β elimination rate constant

[d] $T_{1/2}$ α distribution half-life, $T_{1/2}$ β elimination half-life

[e] AUC area under the curve

subsequent reaction with PEG. In an effort to improve on the PEGylation profile of PAI-2^{C145S} and further control the site of attachment of PEG units, we generated the triple mutant PAI-$2^{C5/145/405S}$ where only a single cysteine at position 161 remained. It has been reported that the attachment of a single large PEG molecule to one site is considered favorable over the attachment of several smaller PEG chains to multiple sites, as uni-site PEGylated proteins are more likely to retain their activity due to the reduced chance of PEG attachment occurring at a receptor binding domain (26). As expected, PEGylation of the triple mutant PAI-$2^{C5/145/405S}$ with 12, 20 or 30 kDa PEG afforded mono-PEGylated protein products in high yield, all of which retained their uPA inhibitory function (Supplementary Information, Fig. S2). However, since disulfide bonds often connect specific structural components of the serpin molecule together and afford enhanced molecular stability (36), the single mutant PAI-2^{C161S}, which contains the C5-C405 disulfide bond and showed an equivalent PEGylation profile to that of PAI-$2^{C5/145/405S}$, was chosen for further pharmacological evaluations.

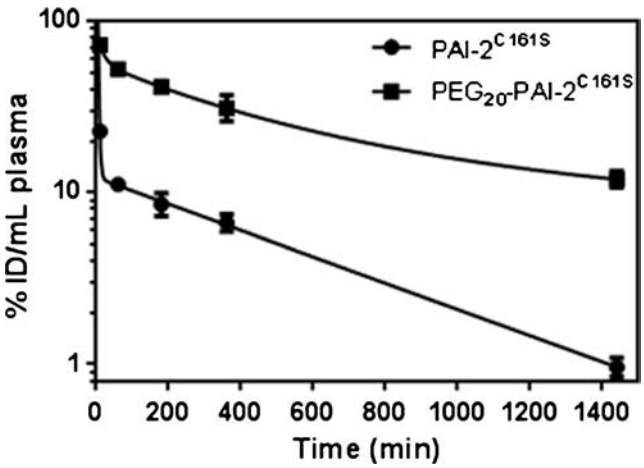

Fig. 5 Plasma clearance profiles of radioiodinated PAI-2^{C161S} and PEG_{20}-PAI-2^{C161S}. Radioactivity in the plasma of mice bearing human breast carcinoma xenografts was measured at 10, 60, 180, 360 and 1,440 min post i.v. administration of ^{125}I-PAI-2^{C161S} or ^{125}I-PEG_{20}-PAI-2^{C161S}. Values shown are the means ($n = 4$) of % ID/mL of plasma corrected for activity remaining in the tail vein ± SEM. The % ID remaining in the tail was always < 5%.

For *in vivo* studies, the 20 kDa PEG moiety was selected to conjugate to PAI-2^{C161S} as a survey of the literature found that the average size of PEG units for FDA approved protein-polymer drug conjugates is 20 kDa (25). Both size and shape of PEG is of major importance in determining tumor targeting characteristics as it has been reported that the relative uptake by tumor tissues is higher than normal tissues when the size of the PEG molecule is greater than 10 kDa (37). Furthermore, PEG with a molecular weight below 40–60 kDa is required to minimize accumulation in the liver (38). We also find no significant difference in the plasma clearance or tissue distribution profiles of 12 kDa and 30 kDa ^{125}I-PEG-PAI-2 conjugates after intraperitoneal administration to non-tumored mice (Supplementary Information, Table S1). The present study compared the BD and PK profiles of ^{125}I-PAI-2^{C161S} and ^{125}I-PEG_{20}-PAI-2^{C161S} in Balb/c nude mice bearing uPA positive, triple negative breast carcinoma xenografts and found the PEGylated protein to yield superior blood residence and tumor accumulation properties. After 24 h, less than 1% of the radioactivity remained in the plasma of mice treated with non-PEGylated PAI-2^{C161S}, while >12 times the activity was detected in the plasma of mice treated with PEG_{20}-PAI-2^{C161S}. This increase in circulation time and hence bioavailability, was found to correlate directly with an increase in the accumulation of activity in the tumor, but most importantly, not in secondary tissues. Such an effect can be attributed to increased molecular size and hydrodynamic radius of the modified protein above the glomerular filtration limit (>60 kDa), leading to reduced renal clearance as well as resistance of the PEGylated proteins to proteolysis, contributing to prolonged plasma half-life (39). A further explanation may be ascribed to the enhanced permeability and retention (EPR) effect. Briefly, due to the accelerated nature of tumor angiogenesis, newly formed tumor vasculature tends to be highly disorganized and hyper-permeable, allowing particles in the range of 10–400 nm to pass through the vessel walls and into the tumor microenvironment (40), whilst the tight endothelium of normal vasculature does not allow such molecules to escape circulation.

In this study we demonstrate that site-directed PEGylation of PAI-2 does not affect the inhibitory activity of the serpin, yet markedly increases circulation time and hence tumor retention after 24 h. Increasing the tissue-specific accumulation of PEG-PAI-2 in the tumor to 10-times that of unPEGylated

Table II Biodistribution (BD) of Radioiodinated PAI-2^{C161S} and PEG_{20}-PAI-2^{C161S} After i.v. Injection in Mice Bearing MDA-MB-231 Breast Tumor Xenografts

		% ID/g of tissue[a]			
	Time (min)	Liver	Kidney	Spleen	Tumor
^{125}I-PAI-2^{C161S}	10	33.46 (±1.58)[d]	49.92 (±2.30)[b]	11.26 (±0.62)[c]	1.37 (±0.09)
	60	9.50 (±0.23)[c]	18.55 (±1.34)	7.12 (±0.30)[b]	4.66 (±0.51)[b]
	180	4.52 (±0.29)	8.14 (±0.49)	4.10 (±0.33)	4.06 (±0.21)
	360	3.72 (±0.23)	6.14 (±0.48)	3.28 (±0.23)	3.18 (±0.38)
	1,440	0.95 (±0.04)	1.08 (±0.04)	0.34 (±0.04)	0.20 (±0.01)[d]
^{125}I-PEG_{20}-PAI-2^{C161S}	10	14.91 (±0.52)	27.52 (±1.05)	6.30 (±0.15)	1.21 (±0.17)
	60	7.23 (±0.31)	14.78 (±1.37)	5.06 (±0.32)	2.62 (±0.19)
	180	5.63 (±0.23)	9.08 (±0.53)	3.82 (±0.22)	3.94 (±0.41)
	360	4.40 (±0.24)	7.28 (±0.42)	3.44 (±0.34)	2.81 (±0.37)
	1,440	1.56 (±0.18)	2.54 (±0.13)	0.94 (±0.08)	1.83 (±0.18)

[a] Values shown are the means ($n = 4$) of % ID/g of tissue corrected for activity remaining in the tail vein ± SEM. The % ID remaining in the tail was always < 5%. [b] $P < 0.01$, [c] $P < 0.001$, [d] $P < 0.0001$ for corresponding timepoint in ^{125}I-PEG_{20}-PAI-2^{C161S} treatments

PAI-2 has the potential to translate to novel drugs with superior efficacy. Since proteins require parenteral administration for systemic delivery, the extended plasma residence time of PEG-PAI-2 may ultimately also translate to fewer injections for therapeutic applications. Furthermore, PEGylation of sulfhydryl groups leaves lysine residues free for conjugation to cytotoxins or radionuclides for therapeutic targeting. We are currently developing such conjugates and in preliminary experiments have successfully conjugated a potent anti-mitotic cytotoxin *N*-alkylisatin (16) to PEG_{20}-PAI-2^{C161S} *via* available amine groups on the surface of the protein and found the conjugate to retain uPA inhibitory and selective cell-killing activities (unpublished observations). Taken together, our results further support the development of PEG-PAI-2 targeted therapies for the treatment of uPA-positive cancers and points to a prospective utility as a non-invasive diagnostic imaging agent.

ACKNOWLEDGEMENTS AND DISCLOSURES

The authors would like to thank the Illawarra Cancer Carers Inc., Kiama, Minnamurra and Gerringong Sunrise Rotary, the Robert East Memorial Fund, Prof. P.Clingan and other private donors for funding assistance. We are also grateful to Mr Benjamin Buckley for assistance with Fig. 1. The authors disclose no conflicts of interest.

Grant Support A University of Wollongong Vice Chancellor's Fellowship, a Cure Cancer Australia Foundation and Cancer Australia project (APP573432) grant to K. L. Vine, and a Cancer Institute NSW Fellowship to M. Ranson are gratefully acknowledged.

REFERENCES

1. Andreasen PA, Kjoller L, Christensen L, Duffy MJ. The urokinase-type plasminogen activator system in cancer metastasis: a review. Int J Cancer. 1997;72(1):1–22.
2. Lund IK, Illemann M, Thurison T, Christensen IJ, Hoyer-Hansen G. uPAR as anti-cancer target: evaluation of biomarker potential, histological localization, and antibody-based therapy. Curr Drug Targets. 2011;12(12):1744–60.
3. Ranson M, Andronicos NM. Plasminogen binding and cancer: promises and pitfalls. Front Biosci. 2003;8:s294–304.
4. Stillfried GE, Saunders DN, Ranson M. Plasminogen binding and activation at the breast cancer cell surface: the integral role of urokinase activity. Breast Cancer Res. 2007;9(1):R14.
5. Carriero MV, Franco P, Votta G, Longanesi-Cattani I, Vento MT, Masucci MT, *et al.* Regulation of cell migration and invasion by specific modules of uPA: mechanistic insights and specific inhibitors. Curr Drug Targets. 2011;12(12):1761–71.
6. Croucher DR, Saunders DN, Lobov S, Ranson M. Revisiting the biological roles of PAI2 (SERPINB2) in cancer. Nat Rev Cancer. 2008;8(7):535–45.
7. Harris L, Fritsche H, Mennel R, Norton L, Ravdin P, Taube S, *et al.* American Society of Clinical Oncology 2007 update of recommendations for the use of tumor markers in breast cancer. J Clin Oncol. 2007;25(33):5287–312.
8. Schmitt M, Harbeck N, Brunner N, Janicke F, Meisner C, Muhlenweg B, *et al.* Cancer therapy trials employing level-of-evidence-1 disease forecast cancer biomarkers uPA and its inhibitor PAI-1. Expert Rev Mol Diagn. 2011;11(6):617–34.
9. Hildenbrand R, Schaaf A, Dorn-Beineke A, Allgayer H, Sutterlin M, Marx A, *et al.* Tumor stroma is the predominant uPA-, uPAR-, PAI-1-expressing tissue in human breast cancer: prognostic impact. Histol Histopathol. 2009;24(7):869–77.
10. Tyndall JDA, Kelso MJ, Ranson M. Inhibitors of the plasminogen activation system – promising new agents for suppressing breast cancer metastasis. In: MCAR, editor. Frontiers in anti-cancer drug discovery. Bentham Science Publishers; 2010. p. 55–78. www.bentham.org/fiacdd.
11. Ngo JC, Jiang L, Lin Z, Yuan C, Chen Z, Zhang X, *et al.* Structural basis for therapeutic intervention of uPA/uPAR system. Curr Drug Targets. 2011;12(12):1729–43.

12. Al-Ejeh F, Croucher D, Ranson M. Kinetic analysis of plasminogen activator inhibitor type-2: urokinase complex formation and subsequent internalisation by carcinoma cell lines. Exp Cell Res. 2004;297(1):259–71.
13. Cochran BJ, Croucher DR, Lobov S, Saunders DN, Ranson M. Dependence on endocytic receptor binding via a minimal binding motif underlies the differential prognostic profiles of SerpinE1 and SerpinB2 in cancer. J Biol Chem. 2011;286(27):24467–75.
14. Croucher D, Saunders DN, Ranson M. The urokinase/PAI-2 complex: a new high affinity ligand for the endocytosis receptor low density lipoprotein receptor-related protein. J Biol Chem. 2006;281(15):10206–13.
15. Croucher DR, Saunders DN, Stillfried GE, Ranson M. A structural basis for differential cell signalling by PAI-1 and PAI-2 in breast cancer cells. Biochem J. 2007;408(2):203–10.
16. Vine KL, Chandran VI, Locke JM, Matesic L, Lee J, Skropeta D, *et al.* Targeting urokinase and the transferrin receptor with novel, anti-mitotic N-alkylisatin cytotoxin conjugates causes selective cancer cell death and reduces tumor growth. Curr Cancer Drug Targets. 2012;12(1):64–73.
17. Vine KL, Locke JM, Bremner JB, Pyne SG, Ranson M. Selective targeting of 2′-deoxy-5-fluorouridine to urokinase positive malignant cells in vitro. Bioorg Med Chem Lett. 2010;20(9):2908–11.
18. Li Y, Rizvi SMA, Ranson M, Allen BJ. Bi-213-PAI2 conjugate selectively induces apoptosis in PC3 metastatic prostate cancer cell line and shows anti-cancer activity in a xenograft animal model. Br J Cancer. 2002;86(7):1197–203.
19. Stutchbury TK, Al-Ejeh F, Stillfried GE, Croucher DR, Andrews J, Irving D, *et al.* Preclinical evaluation of 213Bi-labeled plasminogen activator inhibitor type 2 in an orthotopic murine xenogenic model of human breast carcinoma. Mol Cancer Ther. 2007;6(1):203–12.
20. Lee JA, Cochran BJ, Lobov S, Ranson M. Forty years later and the role of plasminogen activator inhibitor type 2/SERPINB2 is still an enigma. Semin Thromb Hemost. 2011;37(4):395–407.
21. Cochran BJ, Gunawardhana LP, Vine KL, Lee JA, Lobov S, Ranson M. The CD-loop of PAI-2 (SERPINB2) is redundant in the targeting, inhibition and clearance of cell surface uPA activity. BMC Biotechnol. 2009;9:43.
22. Hang MTN, Ranson M, Sauders DN, Liang X-M, Bunn CL, Baker AL. Pharmacokinetics and biodistribution of recombinant human plasminogen activator inhibitor type 2 (PAI-2) in control and tumour xenograft-bearing mice. Fibrinol Proteol. 1998;12:145–54.
23. Ranson M, Berghofer P, Vine KL, Greguric I, Shepherd R, Katsifis A. Different radiolabelling methods alter the pharmacokinetic and biodistribution properties of Plasminogen Activator Inhibitor Type 2 (PAI-2) forms. Nucl Med Biol. 2012;39(6):833–9.
24. Pasut G, Sergi M, Veronese FM. Anti-cancer PEG-enzymes: 30 years old, but still a current approach. Adv Drug Deliv Rev. 2008;60(1):69–78.
25. Kolate A, Baradia D, Patil S, Vhora I, Kore G, Misra A. PEG — a versatile conjugating ligand for drugs and drug delivery systems. J Control Release. 2014;192:67–81.
26. Bailon P, Berthold W. Polyethylene glycol-conjugated pharmaceutical proteins. Pharm Sci Technol Today. 1998;1(8):352–6.
27. Caliceti P, Veronese FM. Pharmacokinetic and biodistribution properties of poly(ethylene glycol)-protein conjugates. Adv Drug Deliv Rev. 2003;55(10):1261–77.
28. Wilczynska M, Lobov S, Ohlsson PI, Ny T. A redox-sensitive loop regulates plasminogen activator inhibitor type 2 (PAI-2) polymerization. EMBO J. 2003;22(8):1753–61.
29. Seyfried BK, Siekmann J, Belgacem O, Wenzel RJ, Turecek PL, Allmaier G. MALDI linear TOF mass spectrometry of PEGylated (glyco)proteins. J Mass Spectrom. 2010;45(6):612–7.
30. Andronicos NM, Ranson M. The topology of plasminogen binding and activation on the surface of human breast cancer cells. Br J Cancer. 2001;85(6):909–16.
31. Pabst TM, Buckley JJ, Ramasubramanyan N, Hunter AK. Comparison of strong anion-exchangers for the purification of a PEGylated protein. J Chromatogr A. 2007;1147(2):172–82.
32. Ranson M, Tian Z, Andronicos NM, Rizvi S, Allen BJ. In vitro cytotoxicity of bismuth-213 (Bi-213)-labeled-plasminogen activator inhibitor type 2 (alpha-PAI-2) on human breast cancer cells. Breast Cancer Res Treat. 2002;71(2):149–59.
33. DeNardo SJ, Yao Z, Lam KS, Song A, Burke PA, Mirick GR, *et al.* Effect of molecular size of pegylated peptide on the pharmacokinetics and tumor targeting in lymphoma-bearing mice. Clin Cancer Res. 2003;9(10 Pt 2):3854S–64S.
34. Harrop SJ, Jankova L, Coles M, Jardine D, Whittaker JS, Gould AR, *et al.* The crystal structure of plasminogen activator inhibitor 2 at 2.0 A resolution: implications for serpin function. Structure. 1999;7(1):43–54.
35. Lobov S, Wilczynska M, Bergstrom F, Johansson LB, Ny T. Structural bases of the redox-dependent conformational switch in the serpin PAI-2. J Mol Biol. 2004;344(5):1359–68.
36. Simonovic I, Patston PA. The native metastable fold of C1-inhibitor is stabilized by disulfide bonds. Biochim Biophys Acta. 2000;1481(1):97–102.
37. Hamidi M, Azadi A, Rafiei P. Pharmacokinetic consequences of pegylation. Drug Deliv. 2006;13(6):399–409.
38. Pasut G, Veronese FM. Polymer drug conjugation, recent achievements and general strategies. Prog Polym Sci. 2007;32:933–61.
39. Chapman AP. PEGylated antibodies and antibody fragments for improved therapy: a review. Adv Drug Deliv Rev. 2002;54(4):531–45.
40. Maeda H, Wu J, Sawa T, Matsumura Y, Hori K. Tumor vascular permeability and the EPR effect in macromolecular therapeutics: a review. J Control Release. 2000;65(1–2):271–84.